Since January 2020 Elsevier has created a COVID-19 resource centre with free information in English and Mandarin on the novel coronavirus COVID-19. The COVID-19 resource centre is hosted on Elsevier Connect, the company's public news and information website.

Biosensors and Bioelectronics 177 (2021) 112971

Contents lists available at ScienceDirect

Biosensors and Bioelectronics

journal homepage: http://www.elsevier.com/locate/bios

Functionalized terahertz plasmonic metasensors: Femtomolar-level detection of SARS-CoV-2 spike proteins

Arash Ahmadivand [a,b,1,*], Burak Gerislioglu [c,1], Zeinab Ramezani [d], Ajeet Kaushik [e], Pandiaraj Manickam [f,g], S. Amir Ghoreishi [h,i]

[a] Department of Electrical and Computer Engineering, Rice University, 6100 Main St, Houston, TX, 77005, United States
[b] Metamaterial Technologies Inc, Pleasanton, CA, 94588, United States
[c] Department of Physics and Astronomy, Rice University, 6100 Main St, Houston, TX, 77005, United States
[d] Department of Electrical and Computer Engineering, Northeastern University, Boston, MA, 02115, United States
[e] NanoBioTech Laboratory, Department of Natural Sciences, Division of Sciences, Art, & Mathematics, Florida Polytechnic University, Lakeland, FL, 33805, United States
[f] Electrodics and Electrocatalysis Division, CSIR-Central Electrochemical Research Institute (CECRI), Karaikudi, 630 003, Tamil Nadu, India
[g] Academy of Scientific & Innovative Research (AcSIR), Ghaziabad, 201 002, Uttar Pradesh, India
[h] Faculty of Electrical & Computer Engineering, Science and Research Branch, Islamic Azad University of Tehran, Tehran, Iran
[i] Department of Electrical Engineering, Varamin (Pishva) Branch Islamic Azad University, Varamin, Iran

ARTICLE INFO

Keywords:
SARS-CoV-2 spike protein
COVID-19 pandemic
Terahertz plasmonic biosensors
Toroidal metasurfaces
Femtomole-level detection

ABSTRACT

Effective and efficient management of human betacoronavirus severe acute respiratory syndrome (SARS)-CoV-2 virus infection i.e., COVID-19 pandemic, required sensitive and selective sensors with short sample-to-result durations for performing desired diagnostics. In this direction, one appropriate alternative approach to detect SARS-CoV-2 virus protein at low level i.e., femtomolar (fM) is exploring plasmonic metasensor technology for COVID-19 diagnostics, which offers exquisite opportunities in advanced healthcare programs, and modern clinical diagnostics. The intrinsic merits of plasmonic metasensors stem from their capability to squeeze electromagnetic fields, simultaneously in frequency, time, and space. However, the detection of low-molecular weight biomolecules at low densities is a typical drawback of conventional metasensors that has recently been addressed using toroidal metasurface technology. This research is focused on the fabrication of a miniaturized plasmonic immunosensor based on toroidal electrodynamics concept that can sustain robustly confined plasmonic modes with ultranarrow lineshapes in the terahertz (THz) frequencies. By exciting toroidal dipole mode using our quasi-infinite metasurface and a judiciously optimized protocol based on functionalized gold nanoparticles (AuNPs) conjugated with the specific monoclonal antibody specific to spike protein (S1) of SARS-CoV-2 virus onto the metasurface, the resonance shifts for diverse concentrations of the spike protein are monitored. Possessing molecular weight around ~76 kDa allowed to detect the presence of SARS-CoV-2 virus protein with significantly low as limit of detection (LoD) was achieved as ~4.2 fM. We envisage that outcomes of this research will pave the way toward the use of toroidal metasensors as practical technologies for rapid and precise screening of SARS-CoV-2 virus carriers, symptomatic or asymptomatic, and spike proteins in hospitals, clinics, laboratories, and site of infection.

1. Introduction

Pioneering efforts in developing reliable and timely recognition of infectious viruses using standard methods date back to the end of the previous century, when intermittent wide-spread epidemics from emerging viruses, such as HIV, severe acute respiratory syndrome (SARS) and Middle East respiratory syndrome coronaviruses (MERS), pandemic influenza H1N1, Ebola and Zika, now SARS-CoV-2 virus associated respiratory syndrome i.e., COVID-19 (Wang et al., 2020; Xiang et al., 2020; Broughton et al., 2020), occurred (Wang et al., 2020; Xiang et al., 2020; Broughton et al., 2020; Kaushik et al., 2016, 2017, 2018). Studies have shown that most of these epidemics derived from

* Corresponding author. Department of Electrical and Computer Engineering, Rice University, 6100 Main St, Houston, TX, 77005, United States.
E-mail address: arash.ahmadivand@metamaterial.com (A. Ahmadivand).
[1] Equal contribution.

https://doi.org/10.1016/j.bios.2021.112971
Received 22 June 2020; Received in revised form 22 October 2020; Accepted 4 January 2021
Available online 6 January 2021

the zoonotic animal-to-human transmission incidents (Cucinotta and Vanelli, 2020; Shereen et al., 2020). In spite of continuous advancements in the development of novel diagnostic approaches in recent years, on every occasion, dramatic scarcities in rapid and accurate detection of infections have hindered the public health response to the evolving epidemiological threat. Considering COVID-19 pandemic (Wang et al., 2020; Xiang et al., 2020; Broughton et al., 2020; Cucinotta and Vanelli, 2020; Shereen et al., 2020), there have been unceasing efforts to develop sensitive and selective recognition tools using both standard and innovative approaches needed for timely diagnostics of COVID-19. CRISPR–Cas12-based detection (Broughton et al., 2020), quantitative real-time polymerase chain reaction (RT-PCR) (Pan et al., 2020; Li et al., 2020), ELISA (the enzyme-linked immunosorbent assay) (Adams et al., 2020), point-of-care (POC) lateral flow immunoassay test (Nguyen et al., 2019; Visseaux et al., 2020), CT-imaging (Fang et al., 2020), and some hematology parameters are the primary focus for clinical diagnosis of the recent fatal virus. Although the accomplished progress in such a short duration is promising, most of these techniques are subject to common limitations (Mujawar et al., 2020). Firstly, many of the available methods have dramatically long turnaround times and they are quite slow. Secondly, for example, the RT-PCR tests require certified facilities, sophisticated equipment-equipped laboratories, and well-trained personal. Thirdly, in many cases, they suffer from the poor sensitivity, where the detection of a specific virus is recommended at picomolar (pM) concentrations. Finally, testing of specific antibodies against SARS-CoV-2 virus in collected patient's or recovered individual's blood is an invasive approach for the assessment of the disease. Instead, saliva test has just been recommended as a decisive and non-invasive sensing procedure at the very early-stages of the infection (Sabino-Silva et al., 2020; Azzi et al., 2020), which possesses immense potential to be utilized in optical sensors and analogous non-contact devices. Newly, several nanoscale integrated architectures based on optical and electronic systems have been introduced to detect SARS-CoV-2 spike protein with much higher sensitivity, such as photothermal biosensors using gold nanoparticles (AuNPs) aggregates (Qiu-Guangyu et al., 2020; Chen et al., 2020) and gated graphene-enhanced field-effect transistor (FET)-based biosensor (Seo et al., 2020). Generally, most of these devices have assisted reasonably sensitive detection of SARS-CoV-2 virus, in subsequent biological components, needed for COVID-19 diagnostics as a major component of pandemic management. However, there is a continuous demand for on-chip, label-free, selective, repeatable, cost-effective, ready-to-use, and ultrasensitive biosensors.

Focusing on photonics architectures, among diverse types of optical biosensors, plasmonic devices based on quasi-infinite metasurfaces are promising tools that have facilitated precise screening and recognition of diverse biomarkers through substantial field confinement at subwavelength geometries (Sannomiya et al., 2011; Zhang et al., 2017). This intriguing feature allowed the detection of targeted biomolecules in highly diluted solutions at low concentrations (Sannomiya et al., 2011; Zhang et al., 2017; Zeng et al., 2015; Nugroho et al., 2020). As a cornerstone of photonics, artificially engineered plasmonic metasurfaces have stimulated the development of efficient, label-free, non-contact, non-invasive, and non-poisonous, multi-analyte immunosensing tools, devised for rapid and real-time detection of the fingerprints of diverse infections and viruses (Stewart et al., 2008; Kabashin et al., 2009; Brolo, 2012), which are particularly important for the diagnosis of diseases and routine point-of-care (POC) clinical evaluations. Their remarkable advantages aside, most of the presently available optical biosensing and immunosensing instruments dramatically suffer from poor limit of detection (LoD) and moderate precision in the identification of ultralow-weight biomolecules at very low densities (Wang et al., 2019).

Most of these drawbacks have recently been addressed using the concept of toroidal metasensors based on flatland plasmonic structures (Lee et al., 2020; Ahmadivand et al., 2017, 2018, 2019a, 2019b; Gupta et al., 2017). It is shown that these platforms are operating based on the third family of electromagnetic modes, known as toroidal multipoles (Dubovik and Tugushev, 1990; Dubovik et al., 2000). The observation and study of these resonant moments in static form was reported in the middle of the previous century (Zel'Dovich, 1957), which was primarily established based on the physics of elementary particles. Later, the toroidal electrodynamic framework was described based on classical electromagnetism (Ahmadivand et al., 2020b), and subsequently the excitation of strong dipolar modes was realized in three-dimensional (3D) artificial media across the microwave frequencies (Kaelberer et al., 2010; Papasimakis et al., 2016). Driven by the ongoing race to miniaturization, researchers are now able to fabricate toroidal-resonant metadevices in exquisite architectures to function at much longer frequencies (Dong et al., 2012; Gerislioglu et al., 2019; Han et al., 2018; Ahmadivand et al., 2019c). For example, in the THz regime, a common feature of toroidal quasi-infinite metasurfaces is the ability of focusing the incident electromagnetic radiation within a tiny spot. Additionally, by considering Eq. 2 in Ref. (Ahmadivand et al., 2020a), these metamolecules support resonances that possess much higher sensitivity to the refractive index perturbations in the surrounding media. To capitalize on these proof-of-principle developments, newly, practical and accurate screening of envelope proteins of a specific virus (Zika virus envelope protein with the molecular weight of ~13 kDa) and antibiotic molecules (kanamycin sulfate or Kantrex, $C_{18}H_{36}N_4O_{11} \times H_2SO_4$, with the molecular weight of ~600 Da) have been reported based on this technology (Ahmadivand et al., 2017, 2018, 2019a, 2019b). Though the detection of biomolecules with molecular weight less than <600 Da was testified based on bulky 3D metamaterials (*e.g.* hyperbolic metamaterials) at pM densities (Sreekanth et al., 2016), similar performance has never been experienced using conventional structures based on flatland metaphotonics. The low molecular weight of these biomolecules distinctively clarifies the superior performance of these sensors compared to analogous planar metasystems in all frequency ranges. This also verifies that THz toroidal metasensors are qualified candidates for the detection of much heavier hormones and drugs, organisms, enzymes, and envelope proteins at very low concentrations.

In this Letter, to resolve the inherent drawbacks of COVID-19 diagnosis tools *via* detecting SARS-CoV-2 spike protein, we developed a THz plasmonic biosensor device based on toroidal dipole-resonant metamolecules that demonstrates extreme sensitivity to the presence of SARS-CoV-2 spike proteins. Toroidal dipole-resonant metasurfaces exhibit unconventional spectral properties that feature low-radiative losses, low mode volumes, and ultranarrow spectral lineshapes through robust confinement of electromagnetic fields. Using these distinct advantages, we tailored a symmetric multipixel planar metamolecule to support a pronounced toroidal dipole around the sub-THz spectra (~0.4 THz). To improve the binding properties of the targeted biomolecules to the devised metasurface, we introduced functionalized colloidal AuNPs conjugated with the respective antibody and captured the spike proteins present in the sample. Since the proposed configuration is a quasi-infinite platform based on periodic arrays of resonant unit cells, the practical realization of a miniaturized, multiplexed, and on-chip immunobiosensing instrument is possible for a wide range of applications (*e.g.* POC). Ultimately, we evaluated the performance of the sensor device in highly diluted solutions and showed that the implemented tool provides femtomolar (fM)-level detection of SARS-CoV-2 spike proteins.

2. Developed protocol to functionalize AuNPs

A schematic of conducted research workflow is depicted in Fig. 1a. Synthesized surface-functionalized AuNPs colloids, with the average diameter of ~45 nm (see Fig. S1 in Supplementary Information), were utilized with robust covalent conjugation to primary amines (-NH_2) of proteins. For the conjugation of SARS-CoV-2 (2019-nCoV, Rabbit MAb) Spike S1 antibody (Sino Biological Inc.) with the NHS activated AuNPs (1 mL), a reconstitution buffer was prepared by combining 0.1 M of

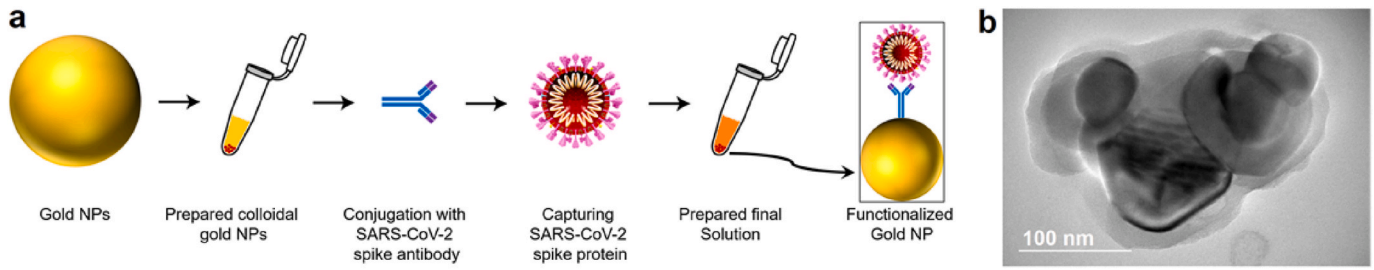

Fig. 1. Functionalization of colloidal AuNPs. a, A schematic for the workflow of the developed functionalized AuNPs conjugated with the respective SARS-CoV-2 antibody and spike proteins. **b**, A TEM image of AuNPs conjugated with the respective antibody of SARS-CoV-2.

reactant buffer with 50 μL of purified antibody. Right after the addition of buffer, the AuNP conjugate was sonicated for 45 s. The solution is incubated while rotating at room temperature for 30 min. Next, 10 μL of quencher was added to deactivate any remaining active NHS-esters. The solution is centrifuged at 5700 rpm for 10 min (at 4 °C). Then, the supernatant is removed cautiously and resuspended with 0.1 mL of reaction buffer. By reiterating the centrifuging process with the same protocol, eventually, conjugate diluent (50 μL) was added and sonicated. The transmission electron microscopy (TEM) image of the functionalized AuNPs bounded with the respective antibody is depicted in Fig. 1b. To prepare the AuNPs with specific antibodies [SARS-CoV-2 (2019-nCoV) Spike S1-His recombinant protein (Sino Biological Inc.)], we used both lyophilized 99% bovine serum albumin (BSA) (Sigma-Aldrich) and pH~7.4 phosphate buffer solution (PBS) to dissolve the immunoreagents. For real-time characterization, after washing the chips with PBS, antibody-modified structures were incubated in PBS containing 0.1 wt % BSA for 30 min. Next, different concentrations of SARS-CoV-2 recombinant spike protein ranging from 2 to 50 fM in PBS was prepared using serial dilution. Once ready, the antibody-functionalized microstructures were rinsed and stored at 4 °C. An optimized time of 20 min was used for the immunocomplex formation at the miniaturized toroidal sensor metasurface. Fig. 1a also contains an artistic picture of the functionalized AuNPs conjugated with the antibody and its subsequent binding with spike protein of SARS-CoV-2 virus.

3. Spectral response of THz metasurface

Fig. 2a shows the schematic representation of the deigned toroidal THz metamolecule (not to scale), adopted from our previous work in Ref. (Ahmadivand et al., 2018), where functionalized AuNPs are dispersed onto the surface of the platform to improve the binding of biomolecules to the metasurface. The geometries of the unit cell are specified in the Supplementary Information (Fig. S2). The numerically and experimentally studied transmission spectra (normalized) of the

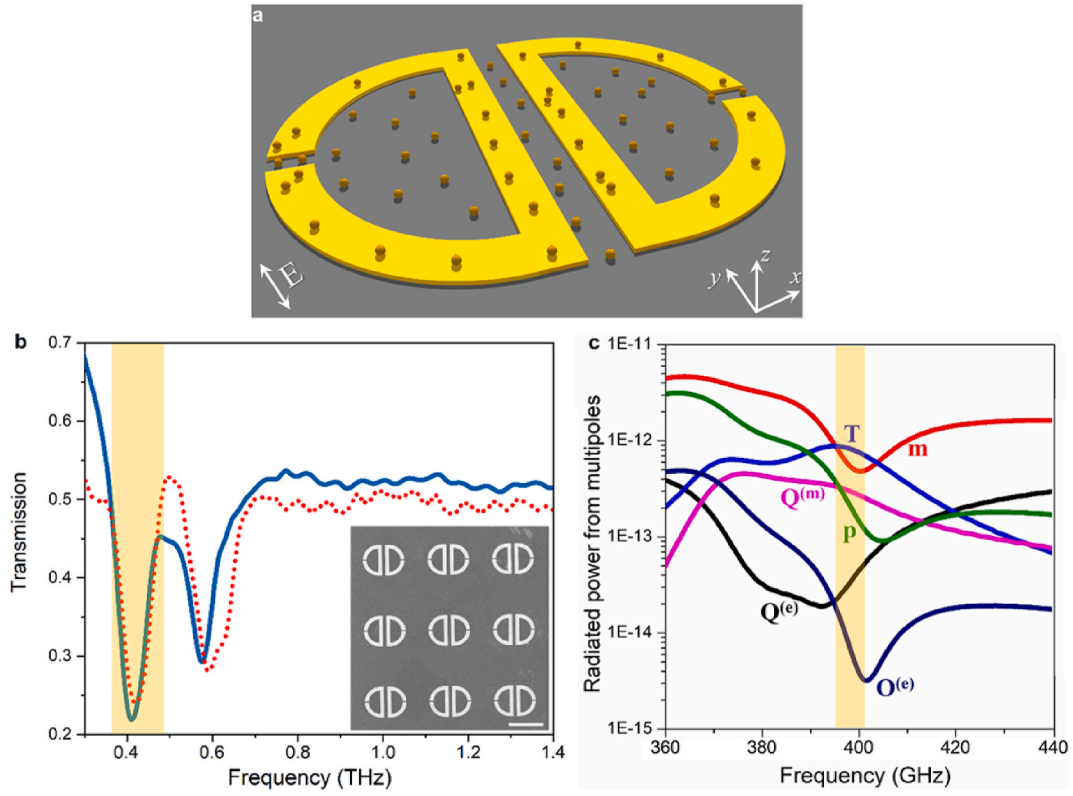

Fig. 2. Simulation, fabrication, and characterization of toroidal THz plasmonic metasurface. a, An artistic rendering of the designed multipixel toroidal unit cell, including the dispersed functionalized AuNPs on top. The polarization direction of the incidence is demonstrated inside the panel. **b**, Numerically calculated (solid) and experimentally probed (dot) transmission spectra of the toroidal metasurface under transverse polarized THz light. The inset is the SEM image of the fabricated metasurface. Scale bar: 100 μm **e**, Theoretically calculated scattered power from individual electromagnetic multipoles induced in the spectral response of metasurface. **p**: electric dipole, **m**: magnetic dipole, $\mathbf{Q^{(e)}}$: electric quadrupole, $\mathbf{Q^{(m)}}$: magnetic quadrupole, **T**: toroidal dipole.

metasurface in the absence of AuNPs are plotted in Fig. 2b. The spectra were obtained through the judicious geometric tuning of the unit cell under transverse-electric (TE) polarized illumination (*s*-polarized beam) to support a distinct toroidal dipole at the sub-THz spectra, around ~0.4 THz. Besides, this profile contains a second minimum around ~0.6 THz correlating with the magnetic dipole mode, which is not related to the scope of this study. It is important to note that colloidal Au NPs are entirely transparent/non-responsive to the incident THz beam, and this results in drastically negligible scattering cross-section radiated from the metasystem. In particular, these functionalized subwavelength metallic particles are exploited to optimize the binding strength between the spike proteins and toroidal dipole-resonant unit cells (Yanik et al., 2010; Xu et al., 2016). The scanning electron microscope (SEM) image of the fabricated planar metasurface is shown in the inset of Fig. 2b, which comprises periodic arrays of engineered Au metamolecules (details on numerical and experimental steps are explained in Supplementary Information). Considering the excitation principle of a toroidal dipole in planar metasurfaces (Ahmadivand et al., 2019d, 2020c; Ahmadivand and Gerislioglu, 2018), we theoretically verified the formation of this mode through vectorial surface current density map to exhibit the required discrepancy between the direction of induced magnetic moments in proximal resonators. In particular, a destructive interference between these oppositely pointed magnetic moments in adjacent resonators leads to the formation of a head-to-tail configuration consisting of a confined arrangement of both charges and currents, which results in the projection of a dynamic toroidal dipole from the scatterer (Fig. S3, Supplementary Information). To provide a full understanding of the excitation of toroidal dipole resonance, we further analyzed the multipole decomposition of an arbitrary vector field by considering the radiated power from electric, magnetic, and toroidal multipoles (Fig. 2c). (Radescu and Vaman, 2003) Noticeably, the toroidal dipole extreme is a dominant contributor to the metasurface response, while the other dipolar and multipolar electromagnetic modes are strongly suppressed.

Another key parameter of the resonant metasurfaces is the confinement of electromagnetic fields by the structured metamolecule. As previously discussed, the ultratight field confinement of toroidal metastructures is a unique feature that enables high sensitivity to the environmental perturbations, analogous to localized surface plasmons-based bio (chemical) sensors (Haes and Van Duyne, 2004; Mayer and Hafner, 2011). Fig. 3a illustrates a cross-cut profile of electric-field (E-field) enhancement as a function of a unit cell length along the *x*-axis, showing a substantial field confinement at the capacitive gap regions in both resonators (see the highlighted regions in the panel). Beyond that, we calculated the 3D E-field enhancement map across the unit cell at the toroidal dipole frequency, validating the strong confinement of plasmons at the capacitive openings (Fig. 3b). These locally generated energetic areas are related to the highlighted regions in the cross-sectional E-field enhancement map in Fig. 3a.

4. Detection of SARS-CoV-2 spike protein

In continue, to highlight the important role toroidal radiations can play in the detection of targeted biomolecules, it is of value to define its response to the presence of SARS-CoV-2 spike proteins bounded to the metasurface, driven by an incident polarized beam. By putting our structured metasurface into practice through dispersing of functionalized AuNPs onto its surface, we conducted a standard evaluation strategy to determine the analytic LoD and sensitivity of the device. To that end, we harnessed a protocol based on a combination of our previously utilized scenario for the diagnosis of Zika virus envelope proteins and screening of Kantrex biomolecules (Ahmadivand et al., 2018, 2019a). For the case of SARS-CoV-2 spike proteins, the assessment of these biomolecules around the toroidal-resonant unit cell is executed by defining the difference between the transmission tensors in absence and presence of spike proteins. Here, we merely considered the tensors correlating with the transmitted and incident electric fields through the metasurface under *s*-polarized beam illumination ($\Delta T(f) \equiv \left|T_{yy}^{\text{Antibody+PBS}}(f)\right|^2 - \left|T_{yy}^{\text{Spike protein}}(f)\right|^2$) (Wu et al., 2012). This model is built on the experimental evolution of the sensing approach. Using this mechanism, the transmission tensor due to SARS-CoV-2 spike proteins can be defined by subtracting following tensors: 1) the transmission tensors for the samples containing the respective antibody plus phosphate buffer solution (PBS), and 2) the same sample with the captured spike proteins. To realize this, we initially determined the reference point for the proposed sensing technique by recording the transmission spectrum of the device *via* injecting PBS to the functionalized AuNPs conjugated with the relevant antibody. Later, we added different concentrations of SARS-CoV-2 spike protein to the solution and measured the variations in the transmittance.

As discussed above, as a control, we primarily prepared 15 μL solution including functionalized AuNPs conjugated with the antibodies selected against SARS-CoV-2 protein and PBS (without the spike protein), then probed the transmission spectra (Fig. 4a, black line). Repeating the same scenario for the samples in the presence of spike proteins, one can characterize the variations in the position of the toroidal dipole. The transmission profile for different concentrations of spike proteins (from 4 to 12 fM) is presented in Fig. 4a, where the AuNPs play the fundamental role of conjugation with antibody, capturing of

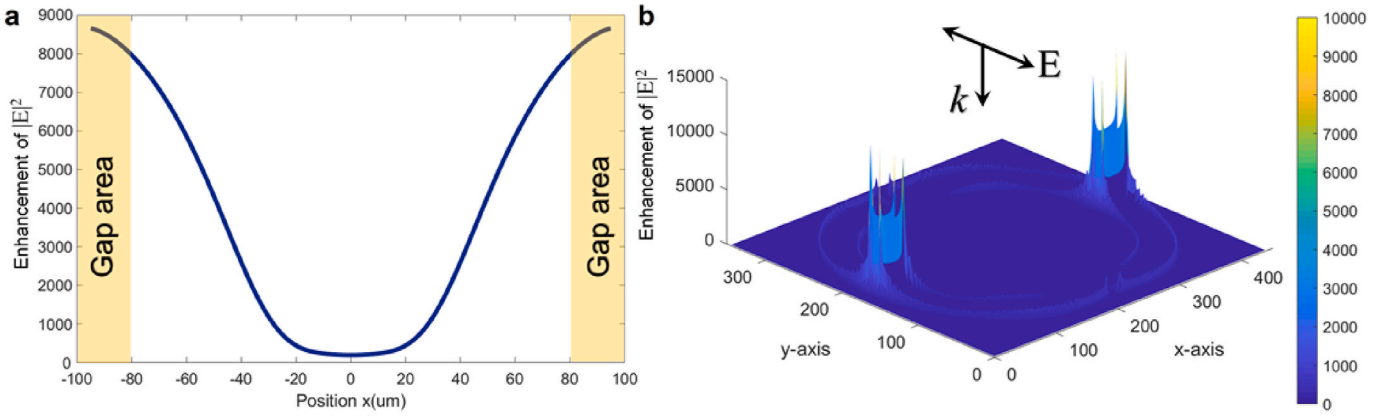

Fig. 3. E-field confinement in the toroidal metamolecule. a, Cross-cut electric field enhancement ($|E|^2$) as a function of position along *x*-axis, simulated for a unit cell at the toroidal dipole frequency, showing significant intensity of the confined fields at the capacitive openings in each resonator. **b**, 3D E-field enhancement map at the frequency of toroidal dipole, in which the strong field confinement was spotted at capacitive gap regions. The polarization and incident light direction are indicated inside the panel.

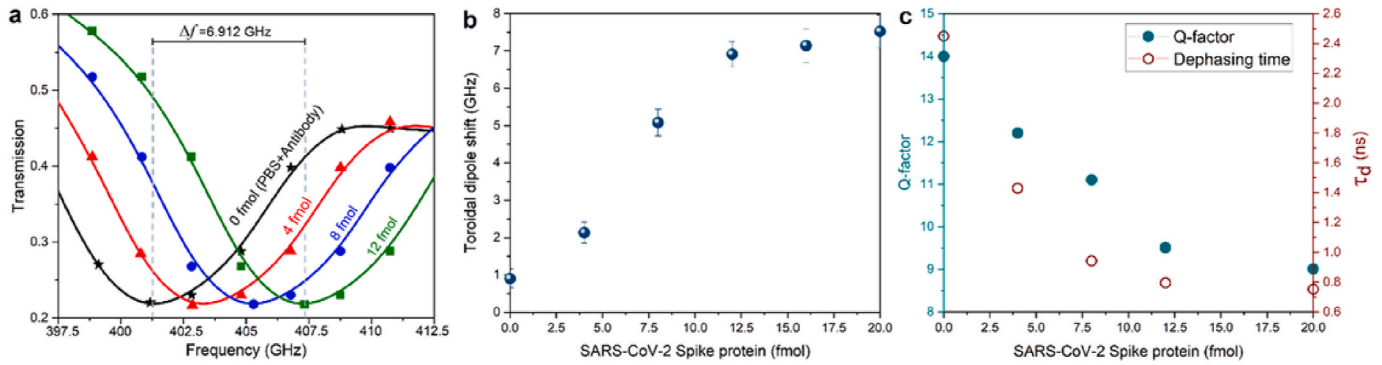

Fig. 4. Evaluation of metasensor performance using functionalized AuNPs and captured spike proteins. a, Measured transmission spectra of the THz metasensor device for different concentrations (4–12 fM) of SARS-CoV-2 spike protein. For 0 fM of spike protein, the spectral response was defined merely for antibody conjugated AuNPs plus PBS. **b**, Variations of the toroidal mode frequency shift for different concentrations of injected spike proteins captured by relevant antibody ranging from 2 to 20 fm **c**, The *Q*-factor and dephasing time (τ_d) of the toroidal lineshape as a function of protein concentration.

proteins, and binding with the resonant unit cells. Here, we observed a traditional and slight red-shift in the position of dipolar mode owing to surface chemistry. On the other hand, by dispersing the spike proteins onto the metasystem, we observed a notable red-shift in the toroidal dipole frequency (Fig. 4a), where a frequency shift of 2.12 GHz was observed for 4 fM of spike protein. Continuous increases in the concentration of SARS-CoV-2 spike protein leads to additional red-shifts in the position of the resonance, and for 12 fM, the frequency shift was measured around 6.912 GHz. It is noteworthy to consider that before each introduction of a new concentration of biomolecules, PBS was injected into the samples to remove the unbound or weakly attached spike proteins. Moreover, sensor performance was monitored as a frequency shift by dispersing of AuNPs with different concentrations of spike proteins (from 14 to 20 fM) onto the sensor surface. Nonlinear variation in the frequency shift (Fig. 4b), as a function of the protein density, was observed, which allows to quantitatively determine the corresponding analytic LoD for the sensor around ~4.2 fM based on a 4 times the signal-to-noise ratio (SNR) criterion. Various densities of functionalized AuNPs, including captured spike proteins, ranging from 2 to 20 fM, were dropped and dried on the surface of the devised metasurface in several steps. The demonstrated findings in Fig. 4b indicates the connection between the toroidal dipole shift and the protein concentration, in which 7.52 GHz shift in the position of the toroidal dipole was observed for 20 fM of spike.

Such shifts in the position of toroidal dipole mode when the protein concentration increased accompanies with slight decline in its quality-factor (*Q*-factor). The variations in the *Q*-factor and corresponding dephasing time (τ_d) due to the presence of spike proteins are demonstrated in Fig. 4c. This panel illustrates the impact of the biomolecules in different condensation on the induced toroidal resonance lineshape and the corresponding dephasing time, because of the modified transmission tensor. Using the classical analysis for the calculation of radiative *Q*-factor, this component was defined as the ratio of the toroidal dipole frequency to the full width at the half maximum (δ) of the lineshape ($Q = f_0/\delta$). On the other hand, following equation is used to quantify dephasing time (Klar et al., 1998; Ahmadivand et al., 2016): $\tau_d = 2\hbar/\delta$. In Fig. 5c, we plotted the radiative *Q*-factor and dephasing time variations as a function of SARS-CoV-2 spike protein concentration. Though by increasing the concentration of biomolecules, the linewidth of the toroidal dipole continuously decays, the induced resonance rationally retains its quality at high concentrations. This implies that at the higher densities of biomolecules, the developed metasensor keeps its performance.

Our findings by far raise the intriguing question: whether toroidal THz plasmonic immunobiosensor metasystem can be employed as a promising and precise tool to detect targeted biomolecules in highly diluted samples or not. To address this inquiry, and to qualitatively and qualitatively demonstrate the ultrahigh sensitivity of the implemented metasensor for the detection of spike proteins in extremely dilute solutions, we used a combination of biomolecules composed of high and low molecular weights. This includes targeted spike proteins plus BSA with molecular weights of ~76 kDa and ~66.5 kDa, respectively. Although the molecular weights of both biomolecules are close to each other, this allows to understand the influence of the heavy bio-objects on the sensing performance of the metadevice. Using the same protocol as we developed earlier in this study, we prepared colloidal AuNPs with

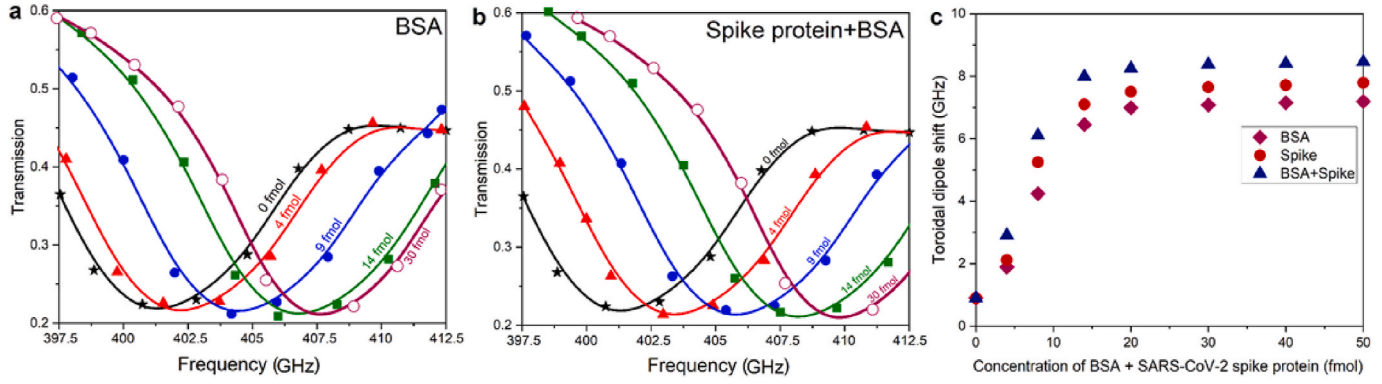

Fig. 5. Evaluation of the THz metasensor in diluted solution. a, **b**, Measured transmission spectra of the THz metasensor device for different concentrations (from 4 to 30 fM) of BSA and SARS-CoV-2 spike protein + BSA, respectively. For 0 fM of spike protein, the spectral response was defined merely for antibody conjugated AuNPs plus PBS. **c,** Variations of the toroidal dipole mode for different concentrations of BSA, SARS-CoV-2 spike protein, and BSA + SARS-CoV-2 spike protein. The spike proteins in all experiments were captured by functionalized AuNPs conjugated with the respective antibody.

different concentrations of BSA and spike protein. To carefully remove the unbounded and weakly conjugated/captured antibody and protein, as well as BSA molecules to the AuNPs, we thoroughly washed the samples before every experiment by distilled water. By introducing functionalized AuNPs solutions to the surface of the metastructure, we probed the transmission spectra as a function of BSA, spike protein, and spike protein + BSA at different concentrations (Fig. 5a and b). Fixing the concentration of biomolecules in all assays between 2 fM and 50 fM, the acquired measurement results for the binding of BSA to colloidal AuNPs show the frequency shift owing to different concentrations of BSA. This is consistent with the observed nonlinear trend of the spike protein in Fig. 4b. It should be underlined that direct measurement of the population of biomolecules on the metasurface is quite challenging, however, we can still define the impact of each biomolecule on the sensing performance quantitatively using the proposed methodology in Ref. (Sreekanth et al., 2016). By considering the shifts in the position of resonance for BSA biomolecules as 4.15 GHz and 6.19 GHz for spike protein at 10 fM, this implies a mean shift per particle which can be approximated as 0.14 GHz and 0.21 GHz, respectively. It should be noted that as the molecular weight of spike protein is almost 1.15 times bigger than BSA, the relatively higher sensitivity going from BSA to SARS-CoV-2 spike protein is significant. Our experimental analyses also revealed that the sensor performance is high at the lowest concentrations, and as can be seen in Fig. 5c, the shift in the position of toroidal dipole reduces dramatically and saturates for further concentrations of biomolecules. Ultimately, we summarized and listed the important parameters and results for the offered metasensor in Table 1. This allows to quantitatively compare the performance of the toroidal metasensor with recently reported similar mechanisms (Mujawar et al., 2020; Azzi et al., 2020) for the detection of SARS-CoV-2 spike proteins.

5. Discussion

The studied toroidal metasensor confirmed to be particularly a proper tool for the precise detection of SARS-CoV-2 spike proteins at extremely low concentrations (down to femto-level densities), with an immense potential to be employed for the implementation of low-cost, selective, repeatable, rapid, and extreme-sensitive modern clinical and pharmacological devices. Similar to its successful counterparts (Wu et al., 2019; Belushkin et al., 2020), the tailored sensing platform enables significant stability and repeatability through the use of functionalized AuNPs. This was experimentally validated in our previous study for the detection of Zika virus envelope proteins based on THz metasensors (Ahmadivand et al., 2018), where the strong binding of AuNPs to the quasi-infinite metasurface allowed for achieving stable and repeatable assays. To verify the longevity of the method, we conducted several measurements using diverse samples with the same concentration of targeted spike proteins. To this end, prepared samples with the antibody were prepared with the described technique in the Methods part above and stored at 4 °C before the measurements. This set of measurements helped us to explore that the developed samples can be used up to five consecutive days with the presence of SARS-CoV-2 spike proteins. The resonance quality remained excellent for five days. In addition, this straightforward bioassay mechanism empowers the detection of biomolecules in a reproducible method with obtained remarkable LoD. Furthermore, short sample-to-result duration around ~80 min is another unique characteristic of the sensing device, which verified that the devised metasensor can be exploited in the detection of SARS-CoV-2 spike proteins as a practical and ready-to-use tool.

Table 1
Important parameters and the obtained results from assays for the plasmonic metasensor.

Sensor device	Plasmonic metasensor [Current approach]	Plasmonic photothermal biosensor (Mujawar et al., 2020)	Gated graphene-enhanced FET based biosensor (Azzi et al., 2020)
Target	SARS-CoV-2 spike protein	SARS-CoV-2 spike protein	SARS-CoV-2 spike protein
LoD	~4.2 fM	0.22 pM	1 fg/mL
Assay components	AuNPs, SARS CoV-2 antibody	AuNPs, SARS CoV-2 antibody	Graphene sheet, SARS CoV-2 antibody
Preparation & Assay reaction time (estimated)	~50 min	>3 h	N/A
Assay sample-to-result time (estimated)	~80 min (including reaction time)	>5 h	>48 h
Assay Results	Qualitative and Quantitative	Quantitative	Qualitative

6. Conclusion

In conclusion, we have developed a highly sensitive miniaturized THz toroidal plasmonic metasensor to detect SARS-CoV-2 spike proteins at femtomole-level concentrations. Our results revealed that introducing functionalized AuNPs to the multipixel metallic metasurface substantially improves the binding strength of biomolecules and subsequently boosts the sensitivity of device. The narrow lineshape, ultratight field confinement, and high sensitivity of toroidal resonances to the environmental perturbations enabled to devise a metasensor platform with unique LoD down to ~4.2 fM. The performance of the plasmonic sensor device was carefully probed in highly diluted solutions containing BSA biomolecules and spike protein. This set of studies proved that the proposed metasensor can be utilized in the detection of SARS-CoV-2 spike proteins in real assays with fairly short sample-to-result duration (~80 min). We envision that the proposed non-invasive, non-contact, and rapid modality in this work allows for the diagnosis of SARS-CoV-2 spike protein at very early-stages with high precision.

7. Outlook

Our developed on-chip and miniaturized SARS-CoV-2 immunosensor based on THz plasmonic toroidal metasurface is able to detect SARS-CoV-2 spike protein selectively at fM densities. Such a sensitive system is required for the early-stage COVID-19 infection diagnostics, assessment of therapy efficacy and generating data with its clinical relevance to manage/understand epidemic. Beyond that, the development of POC system to make COVID-19 infection diagnosis easy at every location will certainly be useful to manage the infection related diseases. The developed metasensor device exhibited excellent performance compared to analogous investigations in the literature, as summarized in Table 1. In future, our aim is to detect SARS-CoV-2 spike proteins at POC after optimizing all the device components i.e., sensing chip (presented in this manuscript), full integration of metachip with microfluidic channel (in progress), and ultimately interfacing of analytical unit with smart display system (in progress). Ultimately sensing COVID-19 using smartphone-based operation. However, the studied and presented sensor device is not yet tested using real samples due to lack of administrative formalities. Serious efforts are being made to establish a collaboration with U.S. based and overseas hospitals to arrange biofluids of COVID-19 infected patient. The results of the complete future studies related with POC sensing of COVID-19 based on plasmonic and photonic metasensors will be published elsewhere.

Authors' contributions

A.A. and B.G. equality contributed, and all other authors contributed extensively to the work presented in this article.

Data availability

All reagents used in this manuscript are available from commercial sources. In addition, the data that support the plots within these paper and other findings of this study are available from the corresponding author upon reasonable request.

Code availability

The written and employed custom codes in FDTD program utilized in this study are available from the corresponding author upon reasonable request.

CRediT authorship contribution statement

Arash Ahmadivand: Conceptualization, Writing - original draft, Software. **Burak Gerislioglu:** Data curation, Writing - original draft. **Zeinab Ramezani:** Investigation. **Ajeet Kaushik:** Supervision. **Pandiaraj Manickam:** Methodology, Validation. **S. Amir Ghoreishi:** Writing - review & editing.

Declaration of competing interest

The authors declare that they have no known competing financial interests or personal relationships that could have appeared to influence the work reported in this paper.

Acknowledgment

P. M. acknowledges the Start-up research grant (SRG/2019/000330) from Science & Engineering Research Board (SERB)-DST, Government of India.

Appendix A. Supplementary data

Supplementary data to this article can be found online at https://doi.org/10.1016/j.bios.2021.112971.

References

Adams, E.R., Anand, R., Andersson, M.I., Auckland, K., Baillie, J.K., Barnes, E., B, J., et al., 2020. Evaluation of antibody testing for SARS-Cov-2 using ELISA and lateral flow immunoassays. medRxiv. https://doi.org/10.1101/2020.04.15.20066407.

Ahmadivand, A., Gerislioglu, B., 2018. Directional toroidal dipoles driven by oblique poloidal and loop current flows in plasmonic meta-atoms. J. Phys. Chem. C 122 (42), 24304–24308.

Ahmadivand, A., Sinha, R., Gerislioglu, B., Karabiyik, M., Pala, N., Shur, M., 2016. Transition from capacitive coupling to direct charge transfer in asymmetric terahertz plasmonic assemblies. Opt. Lett. 41 (22), 5333–5336.

Ahmadivand, A., Gerislioglu, B., Manickam, P., Kaushik, A., Bhansali, S., Nair, M., Pala, N., 2017. Rapid detection of infectious envelope proteins by magnetoplasmonic toroidal metasensors. ACS Sens. 2 (9), 1359–1368.

Ahmadivand, A., Gerislioglu, B., Tomitaka, A., Manickam, P., Kaushik, A., Bhansali, S., Nair, M., Pala, N., 2018. Extreme sensitive metasensor for targeted biomarkers identification using colloidal nanoparticles-integrated plasmonic unit cells. Biomed. Optic Express 9 (2), 373–386.

Ahmadivand, A., Gerislioglu, B., Ramezani, Z., Ghoreishi, S.A., 2019a. Attomolar detection of low-molecular weight antibiotics using midinfrared-resonant toroidal plasmonic metachip technology. Phys. Rev. Appl. 12 (3), 034018.

A. Ahmadivand, R. Sinha, B. Gerislioglu, and N. Pala, Sensor Platform Based on Toroidal Resonances for Rapid Detection of Biomolecules. U.S. Patent 10,288,563, (2019).

Ahmadivand, A., Gerislioglu, B., Ramezani, Z., 2019c. Generation of magnetoelectric photocurrents using toroidal resonances: a new class of infrared plasmonic photodetectors. Nanoscale 11 (27), 13108–13116.

Ahmadivand, A., Gerislioglu, B., Noe, G.T., Kumar Mishra, Y., 2019d. Gated graphene enabled tunable charge–current configurations in hybrid plasmonic metamaterials. ACS Appl. Electron. Mater. 1 (5), 637–641.

Ahmadivand, A., Gerislioglu, B., Ahuja, R., Mishra, Y.K., 2020a. Terahertz plasmonics: the rise of toroidal metadevices towards immunobiosensings. Mater. Today 32, 108–130.

Ahmadivand, A., Gerislioglu, B., Ramezani, Z., 2020b. Toroidal Metamaterials: Fundamentals, Devices, and Applications. Springer Nature, Switzerland.

Ahmadivand, A., Gerislioglu, B., Ahuja, R., Mishra, Y.K., 2020c. Toroidal metaphotonics and metadevices. Laser Photon. Rev. Online 1900326. https://doi.org/10.1002/lpor.201900326.

Azzi, L., Carcano, G., Gianfagna, F., Grossi, P., Gasperina, D.D., Genoni, A., Fasano, M., et al., 2020. Saliva is a reliable tool to detect SARS-CoV-2. J. Infect. 81 (1), e45–e50.

Belushkin, A., Yesilkoy, F., González-López, J.J., Ruiz-Rodríguez, J.C., Ferrer, R., Fàbrega, A., Altug, H., 2020. Rapid and digital detection of inflammatory biomarkers enabled by a novel portable nanoplasmonic imager. Small 16 (3), 1906108.

Brolo, A.G., 2012. Plasmonics for future biosensors. Nat. Photon. 6 (11), 709–713.

Broughton, J.P., Deng, X., Yu, G., Fasching, C.L., Servellita, V., Singh, J., Miao, X., Streithorst, J.A., Granados, A., Sotomayor-Gonzalez, A., Zorn, K., 2020. CRISPR–Cas12-based detection of SARS-CoV-2. Nat. Biotechnol. https://doi.org/10.1038/s41587-020-0513-4 (in press).

Chen, Z., Zhang, Z., Zhai, X., Li, Y., Lin, L., Zhao, H., Bian, L., Peng, Li, Lei, Yu, Wu, Yingsong, Lin, Guanfeng, 2020. Rapid and sensitive detection of anti-SARS-CoV-2 IgG using lanthanide-doped nanoparticles-based lateral flow immunoassay. Anal. Chem. 92 (10), 7226–7231.

Cucinotta, D., Vanelli, M., 2020. WHO declares COVID-19 a pandemic. Acta Biomed.: Atenei Parmensis 91 (1), 157–160.

Dong, Z.-G., Ni, P., Zhu, J., Yin, X., Zhang, X., 2012. Toroidal dipole response in a multifold double-ring metamaterial. Optic Express 20 (12), 13065–13070.

Dubovik, V.M., Tugushev, V.V., 1990. Toroid moments in electrodynamics and solid-state physics. Phys. Rep. 187 (4), 145–202.

Dubovik, V.M., Martsenyuk, M.A., Saha, B., 2000. Material equations for electromagnetism with toroidal polarizations. Phys. Rev. E 61 (6), 7087.

Fang, Y., Zhang, H., Xie, J., Lin, M., Ying, L., Pang, P., Ji, W., 2020. Sensitivity of chest CT for COVID-19: comparison to RT-PCR. Radiology 296 (2), 200432.

Gerislioglu, B., Ahmadivand, A., Adam, J., 2019. Infrared plasmonic photodetectors: the emergence of high photon yield toroidal metadevices. Materials Today Chemistry 14, 100206.

Gupta, M., Kumar Srivastava, Y., Manjappa, M., Singh, R., 2017. Sensing with toroidal metamaterial. Appl. Phys. Lett. 110 (12), 121108.

Haes, A.J., Van Duyne, R.P., 2004. A unified view of propagating and localized surface plasmon resonance biosensors. Anal. Bioanal. Chem. 379 (7–8), 920–930.

Han, B., Li, X., Sui, C., Diao, J., Jing, X., Hong, Z., 2018. Analog of electromagnetically induced transparency in an E-shaped all-dielectric metasurface based on toroidal dipolar response. Opt. Mater. Express 8 (8), 2197–2207.

Kabashin, A.V., Evans, P., Pastkovsky, S., Hendren, W., Wurtz, G.A., Atkinson, R., Pollard, R., Podolskiy, V.A., Zayats, A.V., 2009. Plasmonic nanorod metamaterials for biosensing. Nat. Mater. 8 (11), 867–871.

Kaelberer, T., Fedotov, V.A., Papasimakis, N., Tsai, D.P., Zheludev, N.I., 2010. Toroidal dipolar response in a metamaterial. Science 330 (6010), 1510–1512.

Kaushik, A., Tiwari, S., Jayant, R.D., Marty, A., Nair, M., 2016. Towards detection and diagnosis of Ebola virus disease at point-of-care. Biosens. Bioelectron. 75, 254–272.

Kaushik, A., Tiwari, S., Jayant, R.D., Vashist, A., Nikkhah-Moshaie, R., El-Hage, N., Nair, M., 2017. Electrochemical biosensors for early stage Zika diagnostics. Trends Biotechnol. 35 (4), 308–317.

Kaushik, A., Yndart, A., Kumar, S., Jayant, R.D., Vashist, A., Brown, A.N., Li, C.-Z., Nair, M., 2018. A sensitive electrochemical immunosensor for label-free detection of Zika-virus protein. Sci. Rep. 8, 9700.

Klar, T., Perner, M., Grosse, S., Von Plessen, G., Spirkl, W., Feldmann, J., 1998. Surface-plasmon resonances in single metallic nanoparticles. Phys. Rev. Lett. 80 (19), 4249.

Lee, Y.Y., Kim, R.M., Im, S.W., Balamurugan, M., Nam, K.T., 2020. Plasmonic metamaterials for chiral sensing applications. Nanoscale 12 (1), 58–66.

Li, Y., Yao, L., Li, J., Chen, L., Song, Y., Cai, Z., Yang, C., 2020. Stability issues of RT-PCR testing of SARS-CoV-2 for hospitalized patients clinically diagnosed with COVID-19. J. Med. Virol. 92 (7), 903–908.

Mayer, K.M., Hafner, J.H., 2011. Localized surface plasmon resonance sensors. Chem. Rev. 111 (6), 3828–3857.

Mujawar, M.A., Gohel, H., Bhardwaj, S.K., Srinivasan, S., Hickman, N., Kaushik, A., 2020. Aspects of nano-enabling biosensing systems for intelligent healthcare; towards COVID-19 management. Mater. Today Chem. 17, 100306.

Nguyen, T., Bang, D.D., Wolff, A., 2019. Novel coronavirus disease (COVID-19): paving the road for rapid detection and point-of-care diagnostics. Micromachines 11 (3), 306, 2020.

C. Nugroho, F.A.A., Albinsson, D., Antosiewicz, T.J., Langhammer, C., 2020. Plasmonic metasurface for spatially resolved optical sensing in three dimensions ACS Nano 14 (2), 2345–2353.

Pan, Yang, Zhang, Daitao, Yang, Peng, Poon, Leo LM., Wang, Quanyi, 2020. Viral load of SARS-CoV-2 in clinical samples. Lancet Infect. Dis. 20 (4), 411–412.

Papasimakis, N., Fedotov, V.A., Savinov, V., Raybould, T.A., Zheludev, N.I., 2016. Electromagnetic toroidal excitations in matter and free space. Nat. Mater. 15 (3), 263–271.

Qiu, G., Guangyu, Gai, Z., Tao, Y., Schmitt, J., Kullak-Ublick, G.A., Wang, J., 2020. Dual-functional plasmonic photothermal biosensors for highly accurate severe acute respiratory syndrome coronavirus 2 detection. ACS Nano 14 (5), 5268–5277.

Radescu, E.E., Vaman, G., 2003. Toroid moments in the momentum and angular momentum loss by a radiating arbitrary source. Phys. Rev. E 65 (3), 035601.

Sabino-Silva, R., Gomes Jardim, A.C., Siqueira, W.L., 2020. Coronavirus COVID-19 impacts to dentistry and potential salivary diagnosis, Clinic. Oral Investigations 24, 1619–1621.

Sannomiya, T., Scholder, O., Jefimovs, K., Hafner, C., Dahlin, A.B., 2011. Investigation of plasmon resonances in metal films with nanohole arrays for biosensing applications. Small 7 (12), 1653–1663.

Seo, G., Lee, G., Kim, M.J., Baek, S.-H., Choi, M., Ku, K.B., Lee, C.-S., Jun, S., Park, D., Kim, H.G., Kim, S.J., 2020. Rapid detection of COVID-19 causative virus (SARS-CoV-

2) in human nasopharyngeal swab specimens using field-effect transistor-based biosensor. ACS Nano 14 (4), 5135–5142.
Shereen, M.A., Khan, S., Kazmi, A., Bashir, N., Siddique, R., 2020. COVID-19 infection: origin, transmission, and characteristics of human coronaviruses. J. Adv. Res. 24, 91–98.
Sreekanth, K.V., Alapan, Y., ElKabbash, M., Ilker, E., Hinczewski, M., Gurkan, U.A., De Luca, A., Strangi, G., 2016. Extreme sensitivity biosensing platform based on hyperbolic metamaterials. Nat. Mater. 15 (6), 621–627.
Stewart, M.E., Anderton, C.R., Thompson, L.B., Maria, J., Gray, S.K., Rogers, J.A., Nuzzo, R.G., 2008. Nanostructured plasmonic sensor. Chem. Rev. 108 (2), 494–521.
Visseaux, B., Le Hingrat, Q., Collin, G., Bouzid, D., Lebourgeois, S., Le Pluart, D., Deconinck, L., et al., 2020. Evaluation of the QIAstat-Dx Respiratory SARS-CoV-2 Panel, the first rapid multiplex PCR commercial assay for SARS-CoV-2 detection. J. Clin. Microbiol. 58 (8) e00630-20.
Wang, P., Nasir, M.E., Krasavin, A.V., Dickson, W., Jiang, Y., Zayats, A.V., 2019. Plasmonic metamaterials for nanochemistry and sensing. Acc. Chem. Res. 52 (11), 3018–3028.
Wang, C., Horby, P.W., Hayden, F.G., Gao, G.F., 2020. A novel coronavirus outbreak of global health concern. Lancet 395 (10223), 470–473.
Wu, C., Khanikaev, A.B., Adato, R., Arju, N., Yanik, A.A., Altug, H., Shvets, G., 2012. Fano-resonant asymmetric metamaterials for ultrasensitive spectroscopy and identification of molecular monolayers. Nat. Mater. 11 (1), 69–75.
Wu, Y., Meng, Y., Yakupoglu, B., Adams, M., 2019. A metamaterial/liquid-core waveguide microfluidic optical sensor. Sensor Actuator Phys. 300, 111592.
Xiang, Y.-T., Yang, Y., Li, W., Zhang, L., Zhang, Q., Cheung, T., Ng, C.H., 2020. Timely mental health care for the 2019 novel coronavirus outbreak is urgently needed. Lancet Psychiatry 7 (3), 228–229.
Xu, W., Xie, L., Zhu, J., Xu, X., Ye, Z., Wang, C., Ma, Y., Ying, Y., 2016. Gold nanoparticle-based terahertz metamaterial sensors: mechanisms and applications. ACS Photonics 3 (12), 2308–2314.
Yanik, A.A., Huang, M., Kamohara, O., Artar, A., Geisbert, T.W., Connor, J.H., Altug, H., 2010. An optofluidic nanoplasmonic biosensor for direct detection of live viruses from biological media. Nano Lett. 10 (12), 4962–4969.
Zel'Dovich, Ia B., 1957. Electromagnetic interaction with parity violation. J. Exp. Theor. Phys. 33, 1531–1533.
Zeng, S., Sreekanth, K.V., Shang, J., Yu, T., Chen, C.K., Yin, F., Baillargeat, D., Coquet, P., Ho, H.P., Kabashin, A.V., Yong, K.T., 2015. Graphene–gold metasurface architectures for ultrasensitive plasmonic biosensing. Adv. Mater. 27 (40), 6163–6169.
Zhang, S., Geryak, R., Geldmeier, J., Kim, S., Tsukruk, V.V., 2017. Synthesis, assembly, and applications of hybrid nanostructures for biosensing. Chem. Rev. 117, 12942–13038.